HAL
open science

Structure of single KL0, double KL1, and triple KL2ionization in Mg, Al, and Si targets induced by photons, and their absorption spectra

Yves Ménesguen, Marie-Christine Lépy, Yoshiaki Ito, M. Yamashita, Sei Fukushima, T. Tochio, Marek Polasik, Katarzyna Slabkowska, Lukasz Syrocki, Paul Indelicato, et al.

To cite this version:

Yves Ménesguen, Marie-Christine Lépy, Yoshiaki Ito, M. Yamashita, Sei Fukushima, et al.. Structure of single KL0, double KL1, and triple KL2ionization in Mg, Al, and Si targets induced by photons, and their absorption spectra. Radiation Physics and Chemistry, 2022, 194, pp.110048. 10.1016/j.radphyschem.2022.110048 . cea-03604329

HAL Id: cea-03604329

https://cea.hal.science/cea-03604329v1

Submitted on 10 Mar 2022

HAL is a multi-disciplinary open access archive for the deposit and dissemination of scientific research documents, whether they are published or not. The documents may come from teaching and research institutions in France or abroad, or from public or private research centers.

L'archive ouverte pluridisciplinaire **HAL**, est destinée au dépôt et à la diffusion de documents scientifiques de niveau recherche, publiés ou non, émanant des établissements d'enseignement et de recherche français ou étrangers, des laboratoires publics ou privés.

Distributed under a Creative Commons Attribution - NonCommercial - NoDerivatives 4.0 International License

Structure of single KL^0–, double KL^1–, and triple KL^2–ionization in Mg, Al, and Si targets induced by photons, and their absorption spectra

Y. Ménesguen[a,*], M.-C. Lépy[a], Y. Ito[b,1], M. Yamashita[c], S. Fukushima[d], T. Tochio[e], M. Polasik[f], K. Słabkowska[f], Ł. Syrocki[f], P. Indelicato[g], J. P. Gomilsek[h], J. P. Marques[i], J. M. Sampaio[i], J. Machado[j], P. Amaro[j], M. Guerra[j], J. P. Santos[j], F. Parente[j]

[a] *Université Paris-Saclay, CEA, LIST, Laboratoire National Henri Becquerel (LNE-LNHB), F-91120 Palaiseau, France*
[b] *ICR, Kyoto University, Gokasho, Uji, Kyoto 611-0011 Japan*
[c] *HIT, 3-1-12 Yukihira, Suma-ku, Kobe 654-0037, Japan*
[d] *Kobe Material Testing Laboratory Company, Ltd.,47-13 Nijima, Harima-cho, Kako-gun, Hyogo 675-0155, Japan*
[e] *1-24-14 Inadera, Amagasaki, Hyogo 661-098, Japan*
[f] *Faculty of Chemistry, Nicolaus Copernicus University in Toruń, Gagarina 7, 87-100 Toruń, Poland*
[g] *Laboratoire Kastler Brossel, Sorbonne Université, CNRS, ENS-PSL Research University, Collège de France, Case 74, 4, place Jussieu, 75005 Paris, France*
[h] *Faculty of Mechanical Engineering, University of Maribor, Smetanova 17, SI-2000 Maribor, Slovenia*
[i] *Laboratório de Instrumentação e Física Experimental de Partículas (LIP) and Faculdade de Ciências, Universidade de Lisboa (FCUL), Lisboa, Portugal*
[j] *Laboratory for Instrumentation, Biomedical Engineering and Radiation Physics (LIBPhys), NOVA School of Science and Technology, NOVA University Lisbon, Monte da Caparica, 2892-16 Caparica, Portugal*

Abstract

We investigated experimentally and theoretically x-ray properties of Mg, Al and Si to assess for new reliable x-ray useful quantities. We measured the KL^0– diagram, and KL^1– and KL^2– satellite lines in Mg, Al, and Si, ionized by photon excitation, using a high-resolution anti-parallel double-crystal x-ray spectrometer. Their energy values, full width at half maxima (FWHM), and relative intensities are obtained by the multiple fitting methods and compared with those reported by other excitation processes. It was found that the relative intensity of Mg and Si KL^1 and KL^2 satellite lines to the KL^0 diagram lines depend on the method used to produce the K hole. The evidence of a new transition between $K\alpha_3$ and $K\alpha_4$ in Mg, Al, and S KL^1 satellite lines is suggested. These x-ray diagram and satellite lines were investigated theoretically and we found that Mg $K\alpha_{1,2}$ diagram lines with hidden satellites are especially in very good agreement with the corresponding experimental ones. Moreover, we also determined the mass attenuation coefficients in a wide energy range covering the K-absorption edge, including a detailed evaluation of the associated uncertainties. From the absorption spectra of Mg and Al, the cross sections of the multi-electron transition processes were estimated and match the theoretical values.

1. Introduction

An ionized atom with a single 1s shell vacancy emits an Auger electron or a photon during the de-excitation process. The energies of the photons emitted in the radiative transitions correspond to the characteristic diagram lines in the K x-ray spectra of the particular element. When the 1s vacancy is accompanied by an additional vacancy in one of the higher atomic shells (called a spectator vacancy), the emitted photon energies are slightly shifted to higher values due to the binding energy shifts of the atomic shells, and correspond to the so-called satellite lines in the K x-ray spectrum. Similarly, when the 1s vacancy is accompanied by one or more X-shell vacancies, $X = L, M, N, ...$, the satellite lines are denoted as KX^N, N being the number of existing X-shell vacancies.

The study of the satellite lines is extremely cru-

*Corresponding author
Email address: yves.menesguen@cea.fr (Y. Ménesguen)
[1] present adress: Rigaku Corporation, 14-8 Akaoji-cho, Takatsuki, Osaka 569-1146, Japan

cial in atomic physics, since they provide information on excitation dynamics, relaxation, and other effects that influence the x-ray emission process. Regarding K transitions, several works were carried out to investigate satellite emissions induced by photon [1–14], proton and heavy-ion [15–25], and electron [26–34] impact, although most of them were focused on a few particular elements or transitions.

The creation of multiple inner-shell vacancies in an atom is actually the dominant feature in the collisions of heavy ions with low-Z atoms. The satellites induced in collisions with protons and heavier ions have been extensively studied in the past. Due to the very strong Coulomb interaction between the projectile and the target electrons, ion-induced x-ray spectra exhibit rich satellite structure with very intense high-order satellites. Satellite lines can be observed also in collisions with protons or electrons but the satellite intensities are much weaker and only the lowest-order satellites can be observed. The $K\alpha L^N$ satellite lines of the ion-induced x-ray spectra are affected by the additional ionization of the outer shells, especially the M shell. Since the KM satellites cannot be resolved from the parent diagram line, M-shell ionization causes energy shifts and asymmetrical shape of the spectral lines. On the other hand, the photon-induced satellites, which are almost exclusively the result of the shake process, are practically free from M-shell contributions. Therefore, the study of photon-induced satellite spectra are most fundamental for these purposes since the measured satellite lines are not contaminated by the contribution of the KM satellites [25]. In photo-absorption, since the incident photon is annihilated during the first interaction, the double K-shell ionization can proceed only through electron-electron interactions [11].

In this work we report energy, full width at half maximum (FWHM), and relative intensity values of $K\alpha$, $K\alpha L^1$, and $K\alpha L^2$ lines, produced by photon excitation, using a high resolution double-crystal x-ray spectrometer. The intensities of various satellite lines, relative to the intensity of the $K\alpha_1$ diagram line, were derived from the experimental emission spectra, in order to be compared with the calculated theoretical values. Moreover, we performed absolute measurements of the total mass attenuation and the K fluorescence yields of the elements to evaluate the satellite cross sections, in order to compare with the same quantities from photo-emission.

2. The X-ray diagram and satellite lines

2.1. Theoretical procedures

2.1.1. The multiconfiguration Dirac-Fock method

The multiconfiguration Dirac-Fock (MCDF) method was used to calculate all the quantities needed to simulate the experimental line profiles, namely level energies and radiation, and radiationless transition probabilities between them. A description of the method can be found elsewhere [35–47]. In this work the needed quantities were obtained using both the MCDFGME code developed by Desclaux and Indelicato [46, 47] and the General-purpose Relativistic Atomic Structure Program (GRASP) package [36, 43, 44]. These two codes are state of the art implementations of the MCDF method and allow for large-scale calculations. In the MCDF method the relativistic Hamiltonian for an N-electron atom is given by

$$H = \sum_{i=1}^{N} h_D\left(i\right) + \sum_{j>i=1}^{N} V_B\left(i,j\right), \tag{1}$$

where

$$h_D(i) = \boldsymbol{\alpha_i} \cdot \boldsymbol{p_i} + (\beta_i - 1) + V_i \tag{2}$$

is the one-electron Dirac Hamiltonian, and $V_B\left(i,j\right)$ describes the sum of Coulomb interaction and Breit interaction between the i-th and the j-th electron. Both codes allow, in different approaches, for the inclusion of important radiative effects such as self-energy and vacuum polarization. Electron correlation can also be included. Atomic N-electron wavefunctions for state s, characterized by the total angular momentum J, the projection value of angular momentum M, and parity p, are given in the form [35]

$$\Psi_s\left(JM^p\right) = \sum_m c_m\left(s\right)\Phi\left(\gamma_m JM^p\right), \tag{3}$$

where $\Phi\left(\gamma_m JM^p\right)$ are N-electron configuration state functions (CSFs) built from one-electron four-component Dirac spinors, $c_m\left(s\right)$ are the configuration mixing coefficients for state s, and γ_m contains all information necessary to uniquely define the respective CSFs.

Radiative transitions are obtained in the MCDFGME code including full relaxation using the so-called optimal level (OL) scheme and the Löwdin formalism ensure orthogonality [48]. For radiationless transitions, we assumed that the creation of

the inner-shell hole is independent of the decay process. In the MCDFGME code, the continuum-electron wavefunctions are obtained by solving the Dirac-Fock equations with the same atomic potential of the initial state, and to ensure orthogonality in these calculations, no orbital relaxation was allowed between the initial and final bound state wavefunctions.

In order to obtain *ab initio* $K\alpha_{1,2}$ profiles, we used the MCDFGME code in the single-configuration approach, with the Breit interaction and the vacuum polarization terms included in the self-consistent field process, and other QED effects included as perturbations.

The improvement of high-resolution spectrometers has created a pressure on atomic structure theory to be able to produce reliable, low-uncertainty transition rates and energies in order to reproduce all the features in the experimental spectra. In fact, high-resolution spectrometers such as the one used in this work can provide insight on the chemical state of a given sample solely through the shape of the emission (or absorption) spectra. This means that there are obvious limits to how well experimental spectra, such as the ones presented here, can be simulated from first principles using only the multi-configuration Dirac-Fock formalism, as it describes only isolated atoms. Nevertheless, the discrepancies can be helpful in understanding some solid state effects especially when combined with data from other techniques and/or theoretical frameworks.

2.1.2. Line energies and shapes

We define the width of an atomic level i by the sum of all allowed radiative $R^R_{if'}$ and radiationless $R^{NR}_{ik'}$, transition probabilities from this level to all lower-energy levels, multiplied by $\hbar$ [49],

$$\Gamma_i = \hbar \left(\sum_{f'} R^R_{if'} + \sum_{k'} R^{NR}_{ik'} \right). \tag{4}$$

Here the index f' represents all final one-hole levels resulting from the radiative decay of the initial level i, and the index k' represents all final two-hole levels resulting from the radiationless decay of the same level. The width of a particular transition is given by the sum of the widths of the initial and final levels, as

$$\Gamma_{A-B} = \frac{\sum_{if} g_i \Gamma_{if}}{\sum_i g_i}, \tag{5}$$

where the sums run over the initial levels i, belonging to the one-hole configuration A, and over the final levels f, belonging to the one-hole configuration B.

For Mg, only one level corresponds to each of the K diagram lines initial and final configurations. For Al, due to the interaction with the outer-shell electron, there are four levels corresponding to the initial K-hole configuration and ten levels corresponding to the final L_{23}-hole configuration, and for Si there are eigth levels corresponding to the initial K-hole configuration and twenty one levels corresponding to the final L_{23}-hole configuration. Thus, a procedure must be used to define the energies of the $K\alpha_{1,2}$ "lines". We used the procedure described in [50]. The energy E_{if} of all individual $i \to f$ transitions belonging to the X "line", from an initial level i, weighted by the corresponding transition probability, W_{if} , yields the average energy of that "line"

$$E_X(i) = \frac{\sum_{f(X)} E_{if} W_{if}}{\sum_{f(X)} W_{if}}. \tag{6}$$

Here $f(X)$ runs over all possible final levels in the radiative de-excitation leading to the X "line", from a specific initial level i. Assuming that all levels of a γ configuration are equally populated, the resulting $E_X(i)$ energies are then weighted by the statistical weight $g(i)$ of level i, leading to the statistical average energy E^{SA}_X for the X "line",

$$E^{\mathrm{SA}}_X = \frac{1}{g(\gamma)} \sum g(i) E_X(i), \tag{7}$$

where $g(\gamma)$ is the statistical weight of the γ configuration.

2.1.3. GRASP calculation

Alternatively, using the GRASP package [36], all the levels (with given quantum numbers) corresponding to the set of initial and final configurations are simultaneously taken into account in the MCDF calculations [37–42] to determine the x-ray line positions and spectra structure. It must be underlined that the application of the relativistic MCDF method, taking into account Breit interaction and two quantum electrodynamics (QED) corrections (self-energy and vacuum polarization), and a finite size nucleus model (with a two-parameter Fermi charge distribution) is crucial to reliably determine the significant atomic parameters with the

highest possible accuracy. However, the use of the EAL (Extended Average Level) scheme causes a large discrepancy of $K\alpha_1$ and $K\alpha_2$ line positions with the experimental ones, the reason being that Dirac spinors favor states that are more numerous (final states for diagram lines). Moreover, the calculations for the relative positions of satellite lines are also distorted because of the lack of compensation of more numerous states. Therefore, we have used the MSAL (Modified Special Average Level) scheme [41], which provides compensation and reproduces experimental spectra with high accuracy.

The MCDF method used in the MSAL version is not fully *ab initio*. This scheme is intended to simulate the shape of satellite lines as well as the shape of diagram lines for open-shell atoms. Because of the problem with the correct identification of the final levels that lead to $K\alpha_1$ and $K\alpha_2$ lines we have chosen an approach in which we have divided energetically $K\alpha_1$ line from $K\alpha_2$ line assuming intensity ratio $K\alpha_2/K\alpha_1$ about 0.5. Average $K\alpha_1$ and $K\alpha_2$ line positions have been calculated as a weighted average in which weight was a transition probability (in Coulomb gauge).

2.2. Experimental methodology

In the present work, we used a Rigaku (3580EKI) double-crystal spectrometer that has a high resolution and the ability to scan a range of 20° to 147° in 2θ angle. The temperature in the x-ray spectrometer chamber is controlled within 35.0± 0.5 °C. [14]. The generator is a rhodium end-window x-ray tube operating at 30 kV and 60 mA, under vacuum of around 5 Pa. The double-crystal spectrometer is set in the symmetric ADP (101) Bragg reflection mode, and the spectra were recorded with a gas $Ar_{90}(CH_4)_{10}$ proportional counter at an angular step of 0.005° in 2θ. We used an accumulation time of 100, 200, and 50 seconds per point for Mg, Al, and Si, respectively.

As the observed lines are a convolution of the instrumental function with the emission line, the true full width at half maximum (FWHM) of the emission line can be determined by a simple subtraction of the instrumental function [12–14, 51]. The samples are metallic plates of Mg, Al, and a wafer of Si, and the vertical slit defines a vertical divergence of 0.573°. Three repetitions were done for each element and the data are presented in Fig. 1, without any correction or smoothing. The energy values from Bearden [52] were taken as starting points for the diagram-line fitting parameters.

2.3. Results and discussion on $K\alpha$ diagram and satellite lines

The fitting results of $K\alpha_{1,2,3,4,5,6}$ lines for elements Mg, Al, and Si, are presented in Table 1. The energy values of the $K\alpha_{1,2}$ diagram lines, together with those of the $K\alpha_{3,4,5,6}$ satellite lines, are determined as the averaged line energies obtained from a fitting procedure with Lorentzian functions. The FWHMs are presented as raw or corrected values (for $K\alpha_{1,2}$ using the Tochio's method [51] and marked by an asterisk), together with other reported data [25, 34, 53, 54]. The uncertainties quoted in Table 1 are only due to the counting statistics resulting from the fitting processes and the systematic errors. To obtain realistic uncertainties, those originating from the energy calibration have to be considered (for example, see [33]).

The fitting process with the Lorentzian functions shown in Fig. 1, for $K\alpha_{1,2}$ diagram and satellite lines, used the procedure provided in IGOR PRO (HULINKS, Inc.) software application. The values of χ_r^2 are indicated in the same figure. In our case, N in χ_r^2 is the number of the fitted data points, corresponding to the number of channels in the spectral measurement. The analysis was performed as follows: first, the photon energy, FWHM, and intensity of the diagram and satellite lines in Mg, Al, and Si were changed without constraints; next, the FWHM of $K\alpha_2$ line was made equal to that of $K\alpha_1$ line, and the intensity of the $K\alpha_2$ line was calculated with the intensity ratio of $K\alpha_2/K\alpha_1$ set to 0.5. From this step of the fitting analysis, a satellite line, $K\alpha_{\mathtt{sat}}$ due to the $[1s3s]$ and/or $[1s3p]$ double-hole, was added in the vicinity of the diagram lines to change the energy value, FWHM, and intensity ratio of this satellite line, and all parameters were fitted except the intensities of the diagram lines. And then, the FWHM of the $K\alpha_1$ and $K\alpha_2$ lines was varied until the smallest value of χ_r^2 was attained. Finally, the energy, FWHM, and intensity of each satellite line were fixed, and the photon energy, FWHM, and intensity of the diagram lines were obtained. The results of these analyses are shown in Table 1. The splitting energy of the $K\alpha_1$ and $K\alpha_2$ spectral lines for the three elements, resulting from the fitting analysis, can also be seen in the same table. Moreover, the contribution of the $[1s3s]$ and/or $[1s3p]$ shake processes was investigated as a hidden satellite (specified as $K\alpha_{\mathtt{sat}}$ in Table 1) within the diagram lines.

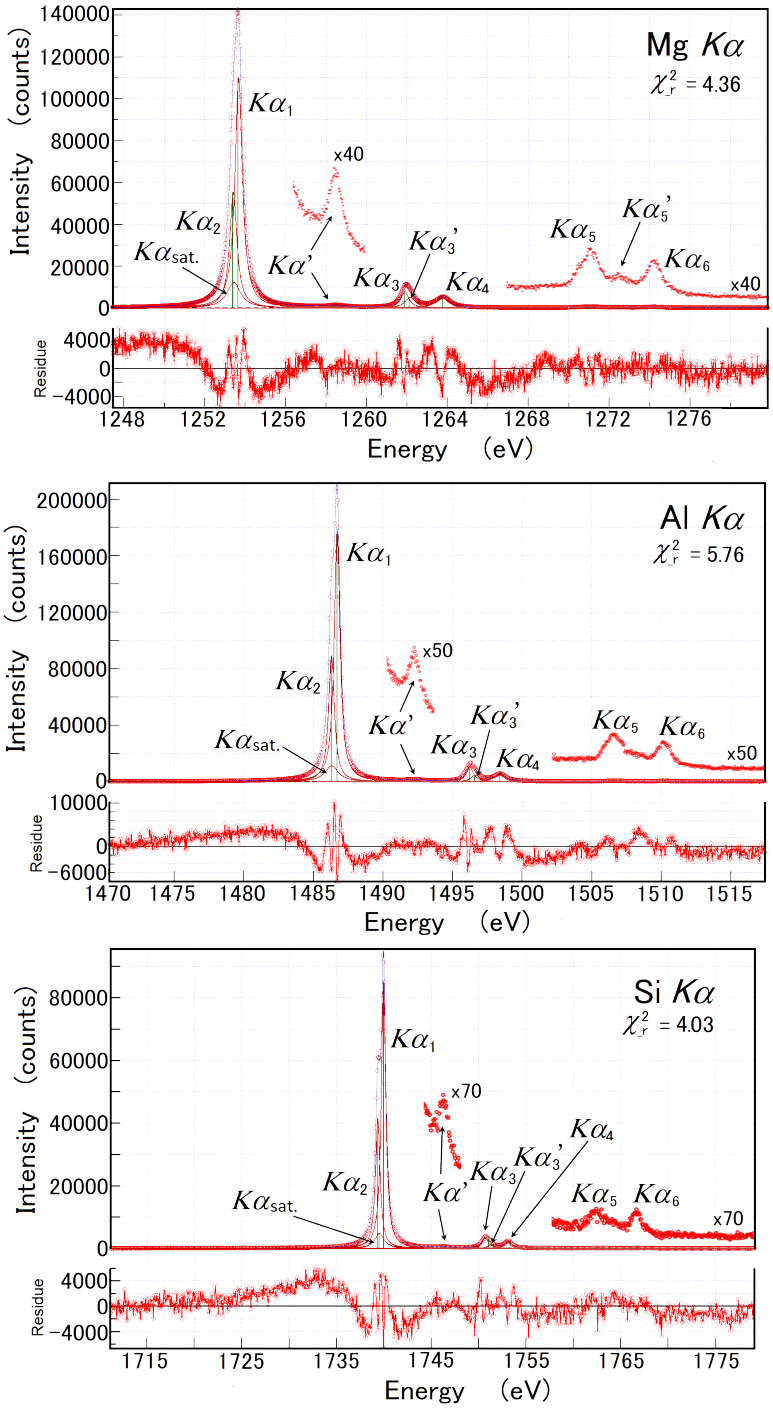

Figure 1: The observed $K\alpha_{1,2}$ diagram lines and satellites of elements Mg, Al, and Si are shown with fitting Lorentzian functions. The spectra were measured using the anti-parallel double-crystal x-ray spectrometer described in detail in [12, 13]. $K\alpha_{3,4,5,6}$ are satellite lines on the high energy side of the $K\alpha_{1,2}$ spectra. A single scan of three repeated measurements is shown for each element together with the value of χ^2_r. Small satellite contributions are magnified. Each hidden satellite, $K\alpha_{\mathtt{sat}}$ was analyzed in the KL^0 diagram line of the elements Mg, Al, and Si, respectively. The green line in each figure indicates the initial value (Bearden's value [52]) for the peak fitting analysis.

Table 1: Mg, Al, and Si observed $K\alpha_{1,2,3,4,5,6}$ line energies, splitting energies ($K\alpha_1$-$K\alpha_2$), full width at half maximum (FWHM), and relative intensities. Corrected FWHMs (CF) have been obtained through Tochio's method [51].

		Energy (eV)					FWHM (eV)		Relat. int. (%)	
		This Work	C&S [53]	Limandri [34]	Schweppe [54]	Kavcic [25]	This Work [CF]	C&P [55]	This Work	Limandri [34]
$K\alpha_1$	Mg	1253.666(16)	1253.56	1253.6	1253.693(12)		0.442(1) [0.380(1)]*	0.36	100	100
	Al	1486.709(5)	1486.72		1486.710(13)		0.493(1) [0.392(1)]*	0.41	100	100
	Si	1739.973(10)	1740.0	1739.98			0.558(1) [0.441(1)]*	0.48	100	100
$K\alpha_2$	Mg	1253.401(17)	1253.56	1253.6	1253.432(13)		0.436(2) [0.374(2)]*	0.36	49.75(19)	
	Al	1486.305(5)	1486.35		1486.298(13)		0.493(2) [0.392(2)]*	0.41	49.4(1.2)	
	Si	1739.361(11)	1739.33	1739.62(1)			0.575(2) [0.458(2)]*	0.48	50.35(26)	
$K\alpha_1 - K\alpha_2$	Mg	0.266(1)	0		0.261					
	Al	0.404(2)	0.37		0.498					
	Si	0.612(1)	0.67	0.36						
$K\alpha_{\mathtt{sat}}$	Mg	1253.422(17)					0.859(32)		19.7(1.3)	
	Al	1486.314(9)					1.117 (49)		16.1(1.4)	
	Si	1739.537(15)					1.199(43)		12.41(89)	
$K\alpha'$	Mg	1258.457(16)	1258.3	1257.66(8)			1.006(28)		1.994(77)	13.5
	Al	1492.306(8)	1493.13				1.162(54)		1.214(98)	
	Si	1746.330(19)	1747.54	1746.4(2)		1746.57(3)	1.18(10)		0.78(11)	0.34
$K\alpha_3$	Mg	1261.887(14)	1261.96	1262.2(1)			0.485(15)		7.97(69)	18.1
	Al	1496.227(1)	1496.35				0.647(41)		7.54(39)	
	Si	1750.687(11)	1751.05	1750.91(3)		1751.10(6)	0.800(24)		5.65(38)	11.1
$K\alpha'_3$	Mg	1262.156(11)					0.585(21)		5.99(76)	
	Al	1496.635(3)					0.685(30)		3.68(41)	
	Si	1751.276(5)	1752.79				0.736(80)		2.03(38)	
$K\alpha''$	Si		1746.1							
$K\alpha_4$	Mg	1263.758(17)	1263.57	1263.7(6)			0.797(7)		8.32(12)	12.6
	Al	1498.397(1)	1498.48				0.932(11)		5.77(13)	
	Si	1753.113(9)	1752.93	1753.22(2)		1753.43(7)	0.931(26)		4.45(18)	3.4
$K\alpha'_4$	Si		1754							
$K\alpha_8$	Mg		1269.1							
	Al		1504.46							
$K\alpha_5$	Mg	1271.034(16)	1271.04	1268.2(4)			1.213(43)		1.228(64)	5.1
	Al	1506.719(22)	1506.82				1.49(10)		0.700(63)	
	Si	1762.677(69)	1763.63	1762.7(2)		1762.75(4)	1.83(25)		0.292(68)	0.4
$K\alpha_7$	Mg	1272.601(24)	1272.5				0.88(14)		0.227(52)	
	Al		1508.46							
	Si		1764.7			1763.67(5)				0.4
$K\alpha_6$	Mg	1274.187(10)	1273.93	1273.4(4)			0.852(35)		0.714(47)	2.2
	Al	1510.212(17)	1510.49				1.069(60)		0.51(18)	
	Si	1766.607(89)	1766.05	1766.3(3)		1767.11(7)	1.05(22)		0.182(50)	0.4

2.3.1. KL^0 ($K\alpha_{1,2}$) spectra of Mg, Al, *and* Si

The synthesized spectra obtained with the MCDFGME code, including the $K\alpha_{1,2}$ diagram and satellite lines for Mg, Al, and Si are presented in Fig. 2, together with the experimental data. The agreement between the two results is very good for Mg, whereas in the Al and Si cases, although the spectral shapes are fairly well in agreement, the peak widths resulting from the theoretical calculations are larger than the experimental ones.

One must take in account that the calculation is performed for independent atoms, whereas the experiment uses metallic samples. Given the fact that the $3p$ orbital is involved in the valence and conduction bands of the metallic samples, some levels that are nondegenerate in an isolated atom will become quasi-degenerate in a solid metallic sample. This fact leads to modifications, not only in the selection rules for the transitions between core-hole states and valence-hole states, but also in their energy. As a result, the multiplet broadening seen in a gas phase x-ray emission spectra should differ from the same x-ray emission from a metallic sample, with the latter having less structure and lower widths. In this case, since the $3p$ electrons are highly involved in the conduction band of these metals, one can see this effect very well as the number of $3p$ electrons increases from Mg (zero $3p$ electrons), to Al and Si (with one and two $3p$ electrons, respectively).

As the multiplet broadening of the emission spectra is not taken into account when computing the line widths from Eq. (5), its value should be closer to the experimental one than the value extracted directly from the emission spectra following the procedure of Guerra *et al.* [56].

The experimental energies of $K\alpha_{1,2}$ diagram lines are presented in Table 1 and Fig. 3. Our experimental results are consistent with those reported by Cauchois and Sénémaud [53], hereafter abbreviated as C & S, and Schweppe *et al.* [54], although a small discrepancy was found for the $K\alpha_2$ line of Mg and Si with the Limandri *et al.* [34] values.

The energy values of $K\alpha_{1,2}$ diagram lines obtained from the theoretical calculations, described in Section 2.1, are shown in Table 2 and also Fig. 3. The energy of $K\alpha_{1,2}$ diagram lines from the MCDFGME calculation (this work) and the calculation by Deslattes *et al.* [57] are larger by about 0.8 eV than the experimental values (see Fig. 3). Both theoretical values result from *ab initio* calculations for isolated atoms and do not include solid state effects.

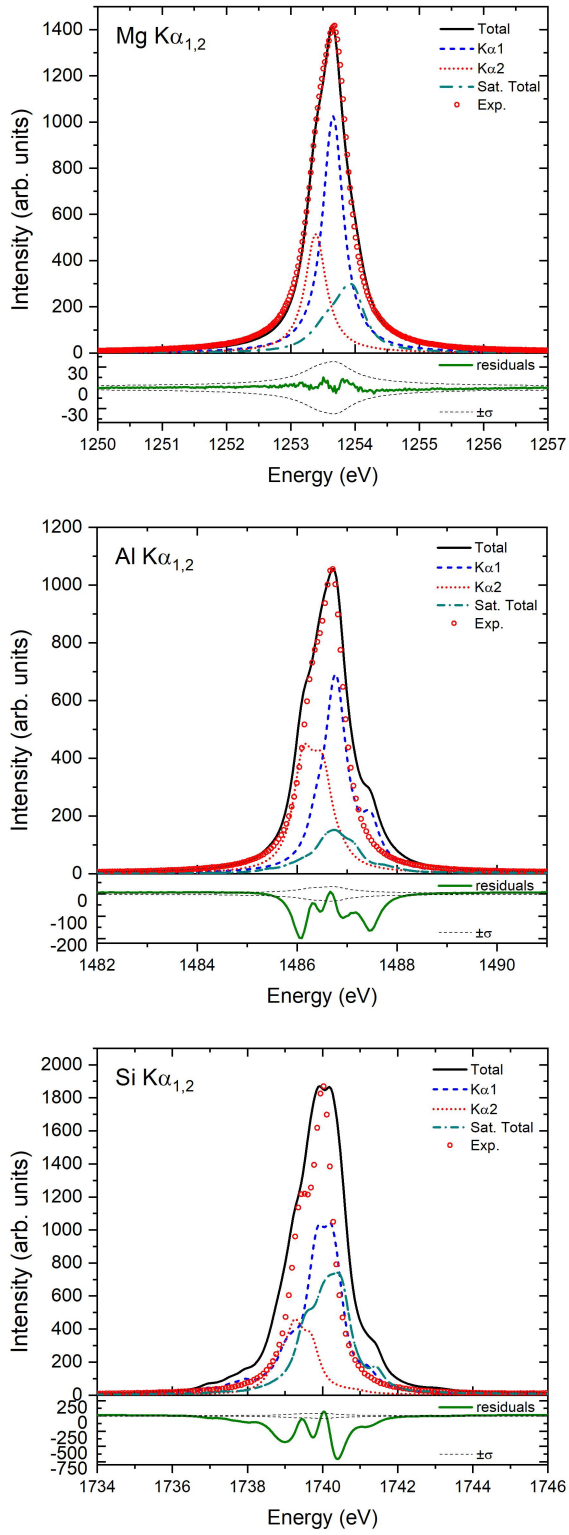

Figure 2: Synthesized profiles, obtained with the MCDFGME code, of Mg, Al, and Si $K\alpha_{1,2}$ lines and satellite bands, together with the experimental data. For each element, an overall energy shift was applied to the theoretical results.

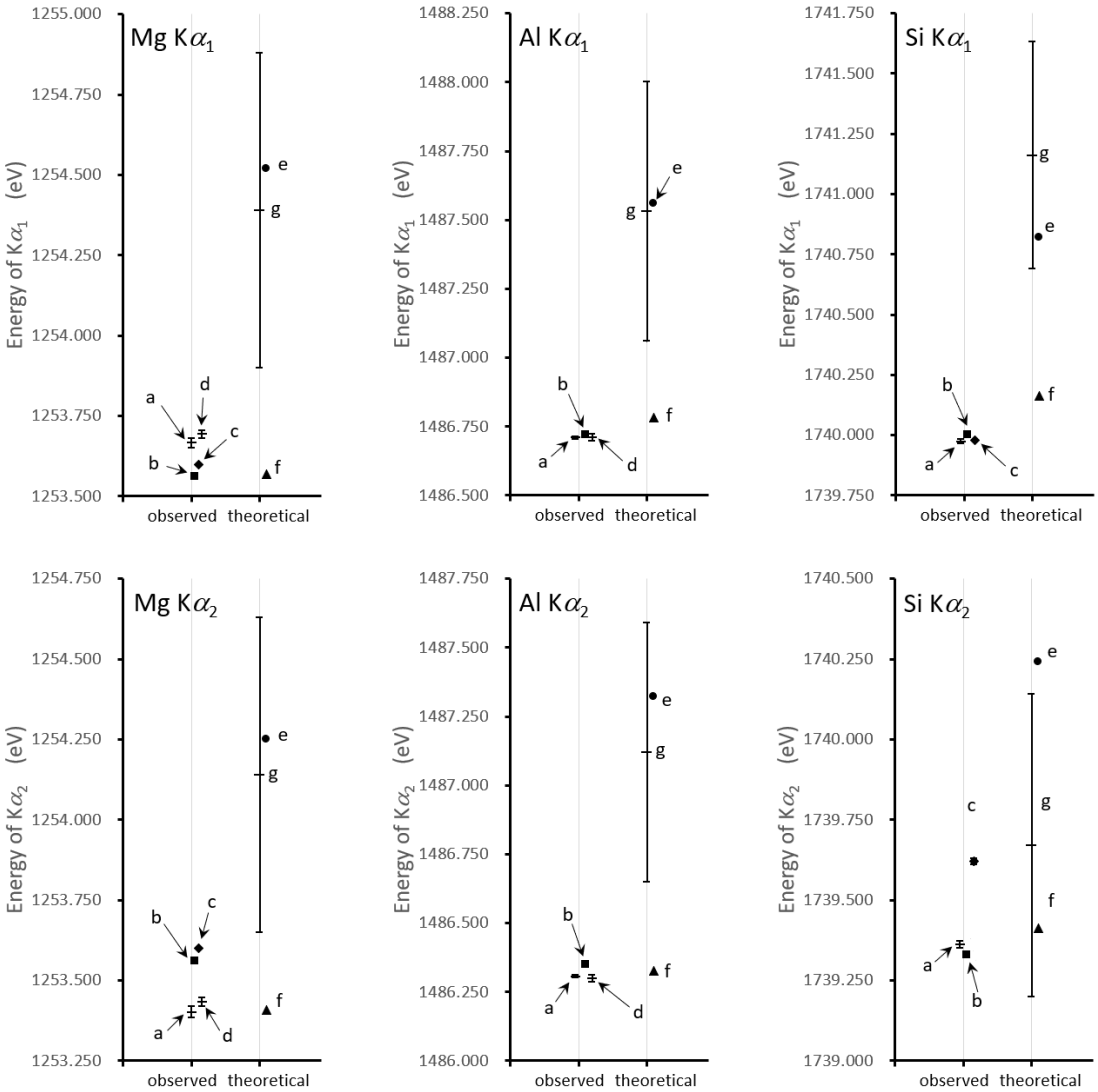

Figure 3: Comparison of the energy values of Mg, Al, and Si $K\alpha_{1,2}$ diagram lines obtained from experiments and theoretical calculations. Experiment: a - this study, b - Cauchois & Sénémaud [53], c - Limandri *et al.* [34], d - Schweppe *et al.* [54]; Theory: e - this study (by MCDFGME), f - this study (by GRASP), g - Deslattes *et al.* [57]. See text for details.

In what concerns the splitting energy ($K\alpha_1$-$K\alpha_2$) in Mg, our experimental value agrees with the value of Schweppe *et al.* [54] but, for Al, it is closer to the values of C & S [53] and Schweppe *et al.* [54], as seen in Table 1, and for Si, there is a small difference with Limandri *et al.* [34] values.

Table 2: Theoretical predictions of $K\alpha_{1,2}$ diagram line parameters (all values in eV).

		MCDFGME		GRASP	Deslattes [57]	Kozioł [49]
		Energy	Width	Energy	Energy	Width
Mg	$K\alpha_1$	1254.52	0.361	1253.57	1254.39(49)	
	$K\alpha_2$	1254.25	0.361	1253.41	1254.14(49)	
	$K\alpha_1$-$K\alpha_2$	0.27		0.16	0.25	
Al	$K\alpha_1$	1487.55	0.379	1486.78	1487.53(47)	0.412
	$K\alpha_2$	1487.29	0.379	1486.33	1487.12(47)	0.412
	$K\alpha_1$-$K\alpha_2$	0.26		0.45	0.41	
Si	$K\alpha_1$	1740.82	0.461	1740.16	1741.16(47)	0.465
	$K\alpha_2$	1740.24	0.461	1739.41	1739.67(47)	0.465
	$K\alpha_1$-$K\alpha_2$	0.58		0.75	1.49	

Concerning the calculated energy values of $K\alpha_{1,2}$ diagram lines and the splitting energies, shown in Table 2, the results from the GRASP-MSAL calculation are in good agreement with the experimental ones (see also Table 1 and Fig. 3), all within ~0.2 eV or less, although the splitting energies from the MCDFGME (this work) and Deslattes *et al.* [57] calculations are consistent, for Mg, with the experimental value. For Al, the splitting energy (0.26 eV) by MCDFGME is smaller than the other values, although the experimental splitting energy values correspond well to the values by GRASP in this study, and to the ones reported by Deslattes *et al.* [57]. The theoretical splitting energy results shown in Table 2, are consistent with the experimental ones (see Table 1), except for GRASP result for Mg, MCDFGME results for Al, and Deslattes *et al.* [57] result for Si.

The linewidths of the Mg, Al, and Si $K\alpha_1$ and $K\alpha_2$ diagram lines, calculated in this work with the MCDFGME code are presented also in Table 2, together with the values of Koziol [49], for Al and Si. This author also used a version of the GRASP code (GRASP2K [44]). It should be emphasized that all theoretical linewidth (shown in Table 2) agree well with our corrected experimental linewidth (see CF in Table 1).

The measured FWHMs of the Mg, Al, and Si $K\alpha_1$ and $K\alpha_2$ diagram lines, corrected for the instrumental broadening, are presented in Fig. 4, together with the $K\alpha_{1,2}$ linewidths of the $3d$ elements measured with the same x-ray spectrometer [12, 14], in order to investigate a systematic trend of the natural FWHM in elements. Several attempts hitherto have been made to obtain a physical interpretation of the observed Z dependence of the lines characteristic parameters, such as the width and asymmetry index, over a wide atomic number range. Ito *et al.* [12] suggested that an asymmetric index in $K\alpha_1$ diagram line in $3d$ elements is attributed to $[1s3d]$ shake processes and the $K\alpha_{11}$ line corresponds to the $K\alpha_1$ diagram line. Various width values from previous measurements including $3d$ elements do not include complete corrections for the instrumental function [33]. The advantage of the double-crystal spectrometer setup lies in the fact that the "true" FWHM of the emission line can be determined, using Tochio's method [51], by a simple subtraction of the estimated values from the FWHM of the measured emission line. This approach was employed in this work. As presented in Fig. 4, the general trend of the corrected FWHMs of the $K\alpha_1$ and $K\alpha_2$ lines as a function of Z, including those of Mg, Al, and Si, is well reproduced by the recommended values based on experimental results of Campbell and Papp [55] (hereinafter abbreviated as CP) and the semi-empirical ones reported by Krause and Oliver [58] (hereinafter abbreviated as KO).

We determined the corrected FWHM values (CF) for both $K\alpha_1$ and $K\alpha_2$ diagram lines for Mg, Al, and Si from the observed FWHM, through Tochio's method [51]. As seen in Fig. 4, the CF values of the $K\alpha_{1,2}$ lines are well consistent with those of the $K\alpha_{1,2}$ from CP and KO, respectively. Moreover, from the fitting analysis of the $K\alpha$ spectral lines in the same elements, the observed splitting energies between $K\alpha_1$ and $K\alpha_2$ lines are also shown in Fig. 5. From the extrapolation of the fitting method, the splitting energy D is expressed by the following equation: $\log_{10} D = 5.0622 \cdot \log_{10} Z - 6.0342$, where Z is an atomic number. Using this equation, we deduce the element for which the difference can be considered as approaching to zero: it will be Carbon (Z=6) or Nitrogen (Z=7). Also, there is a branch point around the element Mn, as seen in Fig. 5. The reason for this is unknown at present time.

2.3.2. KL^1 ($K\alpha_{3,4}$) and KL^2 ($K\alpha_{5,6}$) satellites of Mg*,* Al*, and* Si

The $K\alpha_{3,4}/(K\alpha_1 + K\alpha_2 + K\alpha_{\mathtt{sat}})$ and $K\alpha_{5,6}/(K\alpha_1 + K\alpha_2 + K\alpha_{\mathtt{sat}})$ intensity ratios obtained by photon excitation are shown in Table 3, together with the results from electron bombardment. Our results for the satellite energies

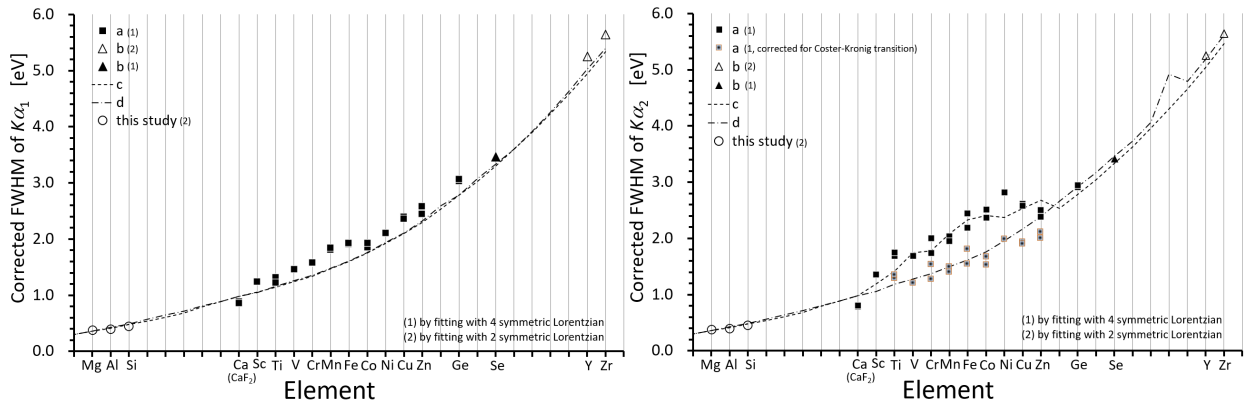

Figure 4: The corrected FWHM of $K\alpha_1$ (left) and $K\alpha_2$ (right) of elements from Mg to Zr including the experimental data in this study. The figures were made using data whose instrumental functions were evaluated using this type two-crystal x-ray spectrometer. a - Ito *et al.* [12], b - Ito *et al.* [13], c - Campbell & Papp [55], d - Krause & Oliver [58].

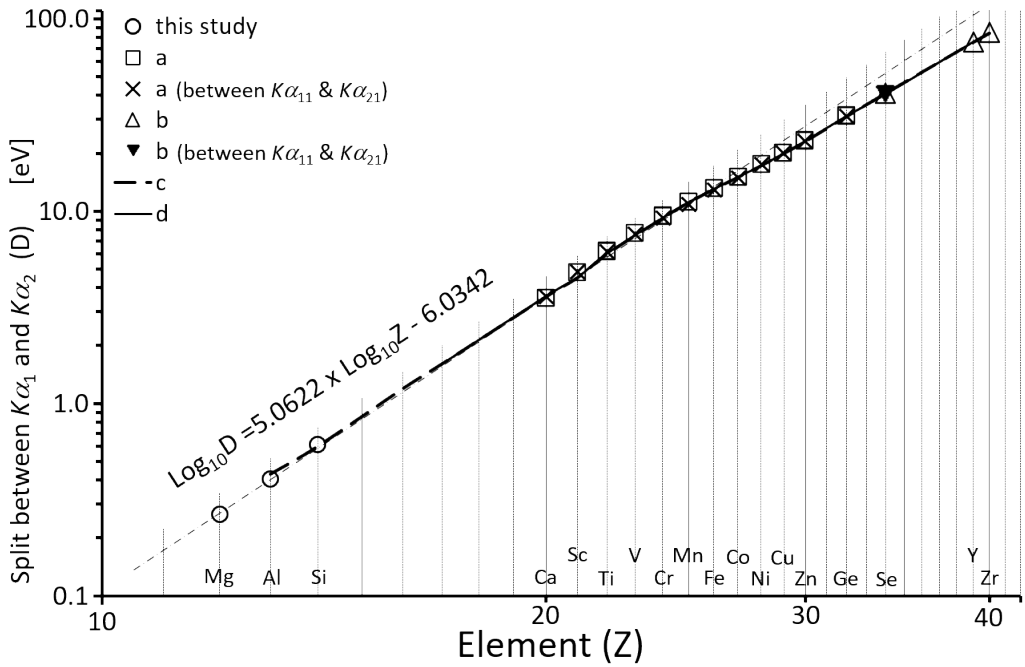

Figure 5: The splitting energy D between $K\alpha_1$and $K\alpha_2$ spectral lines. The function in dashed line represent a fitting. The D in this study are presented by open circles. Using these D values, the fitting function, $\log_{10}D$, was obtained in order to deduce the atomic number Z for $D \sim 0$. a - Ito *et al.* [12], b - Ito *et al.* [14], c - Bearden [52], d - Bearden & Burr [66].

are consistent with those reported by Limandri [34] and Kavčič [25] (see Table 1). Also, as seen in the same table, a new transition named $K\alpha_3'$ was confirmed between $K\alpha_3$ and $K\alpha_4$ in all three elements.

As seen in Table 3 for Mg, measured earlier by means of both photons [59–61], and electron bombardment [29, 34, 62, 63], the relative intensity of satellites is slightly smaller in photon excitation than in electron excitation. That is, each value of $K\alpha L^1/\left(K\alpha L^0 + K\alpha_{\mathtt{sat}}\right)$ and $K\alpha L^2/\left(K\alpha L^0 + K\alpha_{\mathtt{sat}}\right)$ in photon excitation is around 14.3% and 1.28%, respectively, except for the data by Mauron *et al.* [64]. These values are in good consistency with the theoretical calculation of Aberg [65]. The values obtained by Krause [63],

Table 3: Relative intensities (in %) of satellite line groups compared with other values found in the literature. $K\alpha_{3,4}$ includes $K\alpha'$, $K\alpha_3$, $K\alpha_3'$ and $K\alpha_4$ satellite lines, $K\alpha_{5,6}$ includes $K\alpha_5$, $K\alpha_6$ and $K\alpha_7$ satellite lines. All the reported intensities are relative to $K\alpha_1 + K\alpha_2 + K\alpha_{\mathtt{sat}}$.

		P	E	P	E	T	E	P	E	P
		This study	Krause [63]	Mauron [61]	Mikkola [29]	Åberg [65]	Limandri [34]	Utriainen [59]	Baun [62]	Parthasaradhi [60]
$K\alpha_{3,4}$	Mg	14.3	15.5	11.4(1)	16.1(7)	13.6	29.5	14.0(3)	18.7	13.9(6)
	Al	11.0	11.1	7.80(8)	10.2(5)				13.0	
	Si	7.93		5.72(3)			9.9		10.2	
$K\alpha_{5,6}$	Mg	1.28	1.65		1.7(1)	1.1	4.9	1.7(2)	1.65	1.4(3)
	Al	0.73	0.89		0.75(5)				0.89	
	Si	0.29					0.5			

P: Photon excitation; E: Electron bombardment; T: Theory.

Mikkola [29], and Baun [62], using electron beam excitation, are larger than those obtained by photon excitation [59, 60]. It can be seen that the intensity of the satellite lines depends on the excitation methods. Moreover, a transition between $K\alpha_5$ and $K\alpha_6$ satellites was confirmed in this study and its energy and FWHM (see Table 1) were obtained using the fitting analysis. It corresponds to the $K\alpha_7$ line observed by C & S [53].

Table 4: Shake probabilities (in %) for 2s, 2p, 3s, and 3p subshells as the result of a sudden 1s vacancy production for Mg, Al, and Si, calculated with MCDF orbitals.

	$2s$	$2p$	$3s$	$3p$
Mg	0.88	8.82	20.6	
Al	0.71	6.50	11.8	15.1
Si	0.58	4.88	7.90	18.2

For Al, despite the scarce available data in Tables 1 and 3, there seems to be no difference between the excitation methods, except for Mauron's data [64]. The available energy and relative intensity values of Si KL satellites are shown in Tables 1 and 3. Kavčič [25] has identified a new transition between $K\alpha_5$ and $K\alpha_6$. According to this author, the intensity of this transition is comparatively strong, compared to the intensity of the $K\alpha_5$ and $K\alpha_6$ satellites. However, neither Limandri et al. [34] nor we could confirm the existence of this transition. Moreover, one can also see that the photon excitation gives a result which is smaller than the one corresponding to the electron excitation, that is, in the case of the photon excitation, each value of $K\alpha L^1/\left(K\alpha L^0 + K\alpha_{\mathtt{sat}}\right)$ and $K\alpha L^2/\left(K\alpha L^0 + K\alpha_{\mathtt{sat}}\right)$ is around 7.93% and 0.29%, respectively. It is remarkable that the dependence of the satellites intensity on the excitation process is considered to be an important contribution to the interpretation of the KL multiple ionization process.

2.3.3. Contribution to Mg, Al, *and* Si KL^0 ($K\alpha_{1,2}$) *diagram lines of* [1s3s] *and* [1s3p] *shake processes*

The shake probabilities have been calculated in the sudden approximation, according to the method of Carlson and Nestor [67], using the overlap integrals between orbitals in the neutral and the one-hole K-shell configurations. In our calculations, we have not included the extrinsic losses and the interference effects discussed in detail in the paper of Kas *et al.* [68]. The obtained results of the [1s2s], [1s2p], [1s3s] and [1s3p] shake probabilities are presented in Table 4. From the values presented in this table, we conclude that the contribution of [1s3s] and [1s3p] shake processes should be taken in account. They lead to hidden satellite lines within the $K\alpha_{1,2}$ diagram lines profiles. The individual FWHM and the relative intensity ratio of $K\alpha_{1,2}$ diagram and satellite lines in the elements Mg, Al, and Si, obtained from the fitting analysis of the $K\alpha_{1,2}$ line structures with Lorentzian functions, are presented in Table 1.

As the [1s3p] shake process does not occur in Mg, we used the results from the fitting analysis of the Mg diagram lines to investigate the contribution of these processes for the $K\alpha_{1,2}$ diagram lines in Al and Si. Table 4 shows that the probability of [1s3s] shake process increases as the atomic number decreases from Si to Mg. We investigated how the contribution of the [1s3s] shake process affects

the profile of the $K\alpha_{1,2}$ spectra in Mg as seen in Fig. 1. From the results of the fitting analysis (Table 1), the relative intensity of $K\alpha_{\mathtt{sat}}$ decreased from 19.7% to 12.4% from Mg to Si. According to theoretical calculations (Table 4), the $[1s3s]$ shake probability decreases from 20.6% to 7.9% from Mg to Si. The contribution of $[1s3p]$ shake probability increases from 15.1% to 18.2% from Al to Si.

The energies of the satellite lines resulting from the contribution of the $[1s3p]$ shake process are considered to be close to the $K\alpha_{1,2}$ diagram lines energies. Therefore, we assume that the intensity of $K\alpha_{\mathtt{sat}}$, obtained by the fitting analysis, partially includes the contribution of the $[1s3p]$ as well as $[1s3s]$ shake processes, except for Mg, where the $K\alpha_{\mathtt{sat}}$ contribution corresponds just to $[1s3s]$ shake process. That is, as seen Table 4, the calculated value was 20.6% and the measured one 19.7%, as seen in Table 1. In Al, the observed value is 16.1%, so about 28% of the $[1s3p]$ shake probability, 15.1%, is included in $K\alpha_{\mathtt{sat}}$. For Si, $K\alpha_{\mathtt{sat}}$ contains about 25% of the $[1s3p]$ shake probability. Since these results were obtained at an excitation voltage of 30 kV for the primary x-ray, the satellite lines were saturated in intensity and these transition processes could not be identified. Essentially, since the excitation energies of $[1s3s]$ and $[1s3p]$ double holes are different, more accurate values of the relative intensities and FWHM of the $K\alpha_{1,2}$ diagram and satellite lines can be obtained by precisely measuring the $K\alpha_{1,2}$ emission spectra, controlling the excitation energy with an insertion device, using synchrotron radiation.

3. The multi-electron transitions from the absorption spectra

The onset of characteristic diagram lines in the photoemission spectra of the element is denoted by a major edge jump in the absorption spectrum, while satellite lines relate to the multielectron photoexcitation (MEPE) features. At energies above the inner shell ionization threshold, two or more electrons can be excited by the impact of the photon, producing spectator vacancies. Probability for the coexcitation of valence electrons is relatively high, up to 10% or even 20% from single electron probability, the corresponding energy thresholds being close to the single ionization threshold. Coexcitation of more tightly bound electrons is less probable by an order of magnitude, because the energy threshold is higher. Cross section for excitation of more than two electrons is even lower.

Above the main edge, the slope of the absorption cross section as a function of energy of the incident photon changes abruptly at the double ionization threshold energy; single ionization with simultaneous promotion of additional electron to bound level is seen as a sudden jump of the cross section at threshold energy, producing a small edge; double excitations to the unoccupied bound levels produce small resonances. These features can be directly observed in spectra of monatomic samples and have been extensively studied in noble gases [69–72]. The resonances cannot be connected to any satellite lines in the general emission spectra: they show just in the narrow excitation energy interval at the resonance.

In absorption spectra of elements in a dense state or compound, a rich structure in the vicinity of the inner shell ionization threshold originates not only from intra-atomic processes, described above, but also from inter-atomic effects [73]. The atoms surrounding the target atom transform, by their charge and coordination, their outer orbitals as well as the potential field in which the photo-ejected electrons move. XANES (X-ray Absorption Near edge Structure) and EXAFS (Extended X-ray Absorption Fine Structure) features due to chemical composition of the sample extend from approximately 10 eV below the edge to 1–2 keV above the edge, with the arbitrarily put division at 40 eV. In absorption spectra of most samples, the structural (XANES, EXAFS) signal is stronger than MEPE signal [74]. Separation of both contributions is not straightforward and in some aspects not even meaningful: modification of valence orbitals by neighbor atoms affects the valence coexcitation process as well.

3.1. *Experimental measurement of mass attenuation coefficients of* Mg, Al *and* Si

The methodology used to determine the mass attenuation coefficients was extensively described in [75–77] and consequently, will not be detailed here. The mass attenuation coefficient, $\frac{\mu}{\rho}$, is the parameter standing for the interaction probability of a photon beam with matter. It depends both on the material and the photon energy and includes the photo-absorption and scattering effects. The overall attenuation of a parallel and monochromatic photon beam at normal incidence through a thin

target follows the Beer-Lambert law, from which the mass attenuation coefficients can be derived,

$$\frac{\mu}{\rho} = \frac{-1}{\rho \times x} \times \ln(\frac{I}{I_0}) = \frac{-A}{M} \times \ln(T), \quad (8)$$

where I and I_0 are the transmitted and incident photon beam intensities, respectively, ρ and x are, respectively, the target density and thickness, μ/ρ is the energy-dependent mass attenuation coefficient, M is the mass of the target, A its area, and T is the transmission ratio. The procedure using a monochromatic photon beam of low divergence is a convenient way to determine this parameter. In this approach, the final uncertainty budget is linked to the target characteristics and the photon flux intensities.

The experimental transmission measurements were done in an energy range covering the K absorption edges using the two branches of the SOLEIL metrology beamline, the hard x-ray branch from 3 keV to 35 keV, the XUV branch from 0.1 keV to 1.8 keV, and the laboratory source SOLEX for energies between 1.8 keV to 3 keV. At the SOLEIL synchrotron (France), the metrology beamline optics were aligned as described in [75] to minimize harmonics and stray light, and the Bragg angle was calibrated with respect to K-absorption edges of pure metal foils. The Bragg angular position is equipped with an optical encoder and only one calibration point is needed. Therefore, the K-absorption edge of zirconium was chosen for calibration of the Bragg angle of the two-crystal Si(111) monochromator (hard x-ray branch) and aluminum K-absorption edge for the grating at low energies (xuv branch), respectively. At the hard x-ray branch, the transmission measurements were performed using a beam collimated at 3 mm^2 at normal incidence, thus considering the area representative of the average thickness of the whole target.

Transmission measurements were performed within the largest possible energy range with respect to the foil thickness, adapting the energy steps to the features: tens of eV far from the absorption edges and smaller steps of 0.5 eV around the K-absorption edges. The transmitted photon intensities are recorded by means of an AXUV:Al photodiode whose dark noise is subtracted from acquired current values to derive an unbiased transmittance. The laboratory x-ray source SOLEX was also used to cover the energy gap between the hard x-ray and xuv branches using the Si(111) and Béryl(10$\bar{1}$0) crystals as monochromators [78]. The weak flux delivered by this source, compared to a synchrotron beamline, constrained us to use an energy-dispersive spectrometer as detector, which has the advantage of simply discriminating stray light and harmonics at the expense of a higher statistical uncertainty.

3.2. Results

Equation (8) can be modified by including a factor $k_P = 1$, which is responsible for an additional uncertainty due to the elemental purity, calculated as in [75]:

$$\frac{\mu}{\rho} = \frac{-A}{M} \times \ln(T) \times k_P \quad (9)$$

To evaluate the uncertainty of the experimental mass attenuation coefficients, Eq. (9) was derived according to all the influence quantities, as mentioned in the "Guide to the expression of uncertainty in measurement" [79]. The combined standard uncertainty is, thus expressed using the following formula:

$$\left(\frac{u(\frac{\mu}{\rho})}{\frac{\mu}{\rho}}\right)^2 = \left(\frac{u(M)}{M}\right)^2 + \left(\frac{u(A)}{A}\right)^2 + \frac{\left(\frac{u(T)}{T}\right)^2}{\ln(T)^2} + \left(\frac{u(k_P)}{k_P}\right)^2, \quad (10)$$

where the relative uncertainty of the transmission is estimated in the same way as in [75]. Table 5 gives the different contributions to the uncertainty budget of the mass attenuation coefficient measurements. For the mass attenuation coefficients in the soft x-ray range, the different contributions cannot be written in the form of Eq. (10) because mass and area were not measured. Instead, the contributions to the uncertainty budget were obtained from the matching of the different data sets (1.0%).

Accurate values of the sample characteristics are required to derive absolute values of the mass attenuation coefficients. Gadolinium was studied in the form of metal foils, supplied by the Goodfellow corporation, which were chosen with a mass purity better than 99.9%. To derive absolute mass attenuation coefficients from Eq. (8), mass per unit area must be known with the lowest possible uncertainty. The samples were weighed with a calibrated microbalance used in a laboratory whose ambient air hygrometry, temperature and pressure are controlled giving an absolute uncertainty of 9 µg at best. The area was measured with a Mitutoyo

Table 5: Uncertainty budget: relative standard uncertainties of each contributor.

	Mg			Al			Si		
Nominal thickness (µg)	3	50	3000	0.75	6	50	2	20	400
Mass	1.1	0.12	0.001	-	0.37	0.03	-	0.3	0.0032
Area	0.04	0.09	0.04	-	0.04	0.03	-	0.13	0.03
Mass/Area	-	-	-	1	-	-	0.3	-	-
Sample purity	0.6	0.6	0.6	0.4	0.5	0.5	0.1	0.1	0.1
Transmission	0.1	0.13	0.28	0.14	0.17	0.6	0.3	0.3	0.3

QSL-2010Z vision machine consisting of a microscope with two calibrated stages and a picture analyzer. Several foils were used, from 0.75 µm to 50 µm for aluminum and from 3 µm to 3000 µm for magnesium.

The measurements resulted in a set of transmission data for metallic Mg and Al in the photon energy range from 0.3 keV to 26 keV, from which the energy dependent mass attenuation coefficient was calculated, covering the K-absorption edge (Fig. 6).

These results were compared to the EPDL97 database [80]. The relative differences between the present results and the values from EPDL97 are presented in Fig. 6 right. This graph plots the relative deviation as stated in the following equation:

$$\frac{\Delta\mu}{\mu} = \frac{\mu_{EXP} - \mu_{DB}}{\mu_{DB}} \times 100, \tag{11}$$

where μ_{EXP} denotes for the presently measured mass attenuation coefficients and μ_{DB} stands for values from a published database. The largest relative difference found around the K-absorption edge is essentially due to the fine structures which are detailed in the present measurements. The $\frac{\Delta\mu}{\mu}$ deviation plotted for the data from Cullen [80] is within 2% for most energies below 20 keV except for Mg where we found a larger difference for photon energies between 2 keV and 3 keV. At higher energies, the deviations become significant.

3.3. The cross-section of multi-electron transitions

Our absorption experiment was not specifically designed to extract MEPE cross-sections. Nevertheless, some information can be gained on $2p$ coexcitation in Mg and Al (Si was not measured in the region of interest). Valence co-excitations ($3s$ for both elements and $3p$ for Al) are too close to the edge to be recognizable while $2s$ (or even 1s) is too weak.

The IFEFFIT package [81] was used to identify the structural contribution to the absorption signal. Due to limited range and quality of input data, only the first two shells of neighbors could be included in the fitting procedure. Refinement of structural parameters gave a crude estimate of the EXAFS signal with some structural oscillations still remaining (Fig. 7a, b). This estimate was subsequently subtracted from the spectrum. Extraordinary long data regions below and above the edge were exploited (Fig. 8), to determine the average Victoreen trends [82]. Normalized K-edge absorption (Fig. 9) was obtained by a subtraction of the pre-edge Victoreen and then by a division with the difference of both Victoreens. Average energies of the lowermost MEPE thresholds, calculated with Hartree-Fock code [83], are marked in the figure (double excitation to bound states, single ionization with coexcitation to bound state, and double ionization, respectively). There is an apparent jump of absorption in the vicinity of the $2p$ coexcitation thresholds, giving a $2p$ coexcitation probability between 2% and 8% of single electron ionization probability in both Mg and Al, in agreement with our calculated $2p$ shake probabilities (Table 4).

4. Summary and conclusions

In this work we present an approach to elucidate the electronic interactions among Mg, Al, and Si atoms by investigating both emission and absorption spectra.

Mg, Al, and Si KL^0, KL^1, and KL^2 diagram and satellite lines were measured using the anti-parallel double-crystal x-ray spectrometer and analyzed by multiple fitting method. The observed natural line widths of these elements $K\alpha_{1,2}$ spectral lines were

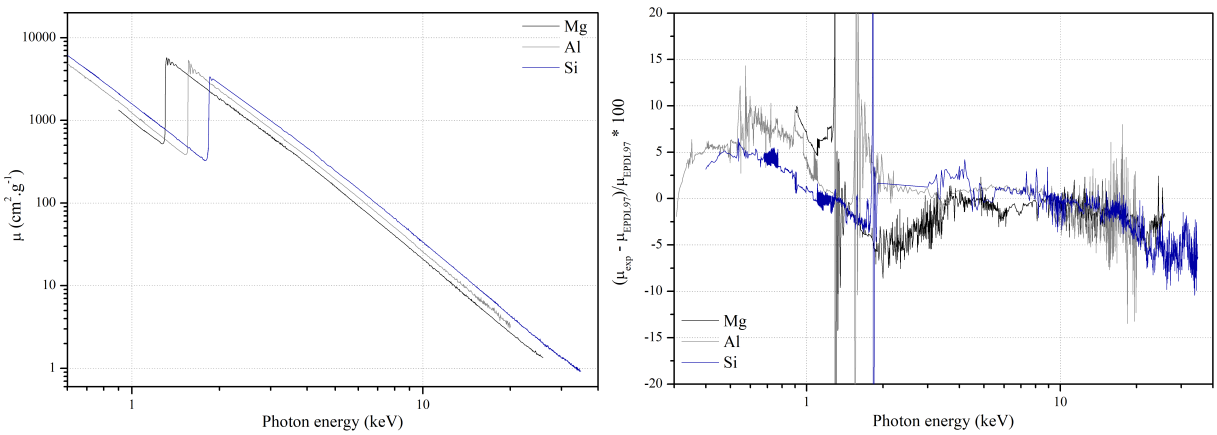

Figure 6: Left: Mass attenuation coefficients of Mg, Al (as metal) and Si measured between 0.3 keV and 35 keV. Right: Comparison of the new experimental values of the mass attenuation coefficients with the data EPDL97 from the literature.

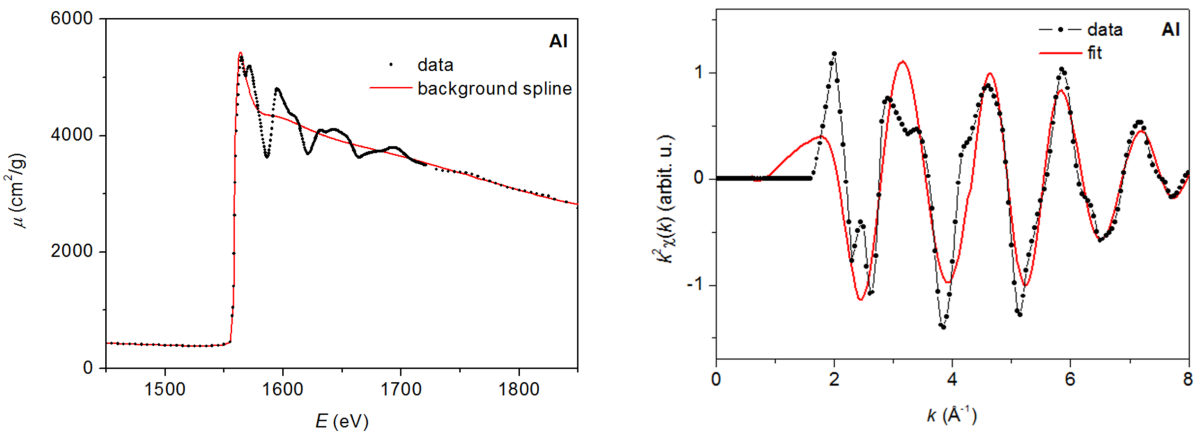

a b

Figure 7: EXAFS fitting in Al. a) Measured data with spline background, b) EXAFS data and fit in k-space, k^2 weighing.

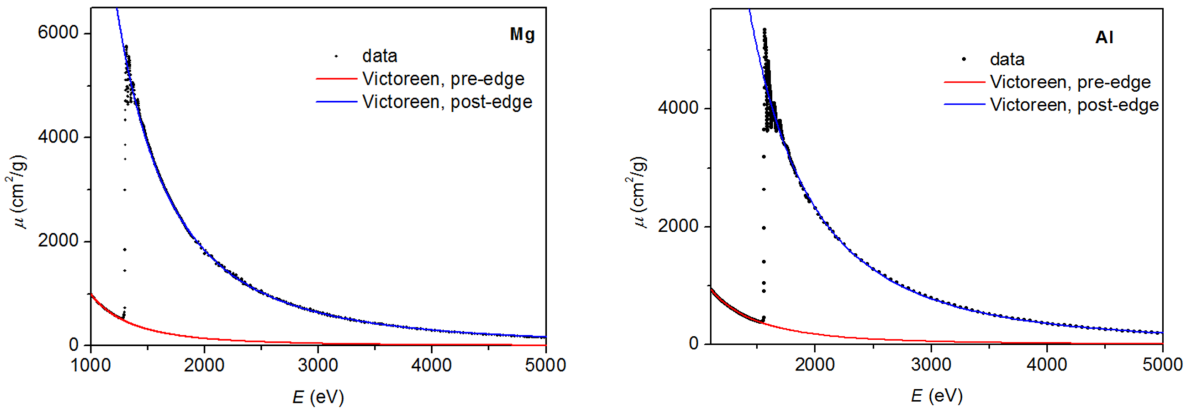

a b

Figure 8: Victoreen trends below and above the K absorption edge in Mg (a) and Al (b).

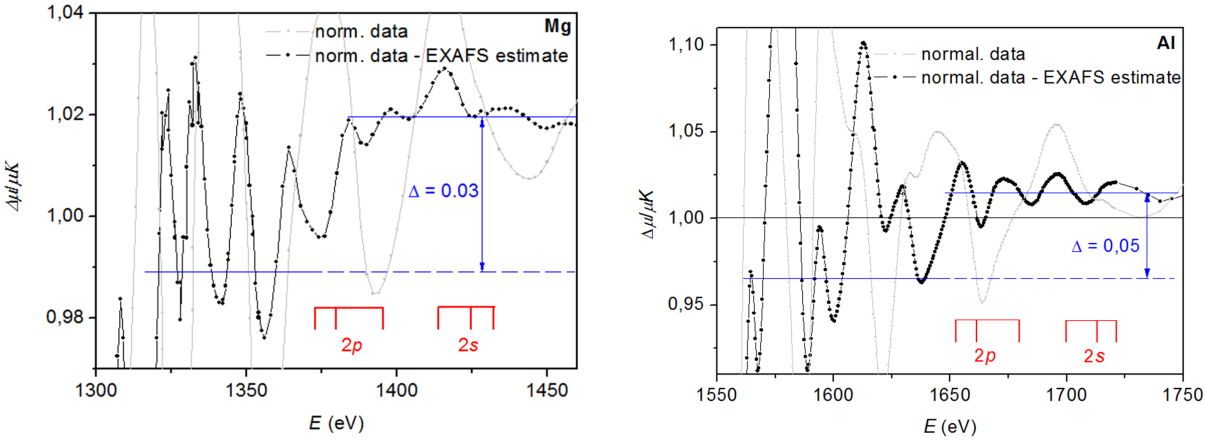

a b

Figure 9: $2p$ MEPE region - normalized data (gray), normalized data with structural oscillations removed by EXAFS model (black)..

found to be consistent with the published recommended ones [55]. The relative intensity of Mg and Si KL^1, and KL^2 satellite lines to KL^0 diagram lines were found to be dependent on the excitation method. It is suggested that there is a new transition between $K\alpha_3$ and $K\alpha_4$ in the KL^1 satellite lines in all three elements studied.

The agreement between the $K\alpha_{1,2}$ experimental spectrum and the synthesized spectra obtained from the theoretical calculations using the MCDFGME code is excellent for Mg (zero $3p$ electrons) but not for Al (one $3p$ electrons) and Si (two $3p$ electrons), where the peak widths resulting from the theoretical calculations are larger than the experimental ones. This is due to the fact that the calculations have been performed for independent atoms, whereas the experiment uses solid metallic samples.

Moreover, from the absorption spectra of Mg and Al, an apparent jump was confirmed in the vicinity of the $2p$ co-excitation thresholds giving the probability between 2% and 8% of single electron ionization probability. The probabilities are in good consistent with our calculated $2p$ shake probabilities. We also measured the mass attenuation coefficients of Mg, Al, and Si in a wide energy range using a well-established methodology, including reliable uncertainties.

5. Acknowledgments

Y. Ménesguen, M.-C. Lépy and Y. Ito acknowledge the financial support for the measurements of a part of the data by the REXDAB Collaboration that was initiated within the International Fundamental Parameter Initiative. This work was also supported by the National Science Centre, Poland under grant number 2017/25/B/ST2/00901 and grant number 2021/05/X/ST2/01664, and by the research center grants UID/FIS/04559/2013 to LIBPhys-UNL, contract UIDP/50007/2020, to LIP, and Project No. PTDC/FIS-AQM/31969/2017 "Ultra-high-accuracy x-ray spectroscopy of transition-metal oxides and rare earths", from FCT/MCTES/PIDDAC, Portugal, and by the Slovenian Research Agency (P1-0112). The Laboratoire Kastler Brossel is Unité Mixte de Recherche du CNRS, de l'ENS et de l'UPMC No. 8552. Y. Ito and J.P.Gomilsek thank Emeritus Prof. A. Kodre for valuable discussions.

References

[1] Graeffe, G., Juslen, H., and Karras, M., 1977. Si K_α X-ray emission spectra of Si, SiC, SiO_2 and Si_3N_4. J. Phys. B: Atom. Mol. Phys. 10, 3219. https://doi.org/10.1088/0022-3700/10/16/017

[2] Chevallier, P., Tavernier, M., and Briand, J. P., 1978. On the natural width of the K_α X-ray line observed at the energy threshold. J. Phys. B: Atom. Mol. Phys. 11, L171. https://doi.org/10.1088/0022-3700/11/6/003.

[3] Babu, G. Ramesh, Gopalakrishna, V., Raju, M. L. N., Parthasaradhi, K., Murty, V. Radha Krishna, Murti,

M. V. R., and Rao, K. S., 1987. Kα x-ray satellites of P, S, C l, K, and Ca excited by photons. Phys. Rev. A 36, 386. https://doi.org/10.1103/PhysRevA.36.386.

[4] Fritsch, M., Kao, C. C., Hämäläinen, K., Förster, E., and Deutsch, M., 1998. Evolution of the Cu K$\alpha_{3,4}$ satellites from threshold to saturation. Phys. Rev. A 57, 1686. https://doi.org/10.1103/PhysRevA.57.1686

[5] Verma, H. R., 2000. A study of radiative Auger emission, satellites and hypersatellites in photon-induced K x-ray spectra of some elements in the range $20 \leq Z \leq 32$. J. Phys. B: Atom. Mol. Phys. 33, 3407. https://doi.org/10.1088/0953-4075/33/17/318

[6] Kawatsura, K., Morikawa, T., Takahiro, K., Oura, M., Yamaoka, H., Maeda, K., Hayakawa, S., Ito, S., Terasawa, M., Mukoyama, T., 2003. Evolution of the Kα x-ray satellites for Fe, Ni and Zn: from threshold to saturation. J. Phys. B: Atom. Mol. Phys. 36, 4065. https://doi.org/10.1088/0953-4075/36/20/001

[7] Galambosi, S., Sutinen H., Mattila, A., Hämäläinen, K., Sharon, R., Kao, C. C., and Deutsch, M., 2003. Near-threshold multielectronic effects in the Cu K$\alpha_{1,2}$ x-ray spectrum. Phys. Rev. A 67, 022510. https://doi.org/10.1103/PhysRevA.67.022510

[8] Shigeoka, N., Oohashi, H., Tochio, T., Ito, Y., Mukoyama T., Vlaicu, A. M., and Fukushima, S., 2004. Experimental investigation of the origin of the Ti $K\alpha''$ satellites. Phys. Rev. A 69, 052505. https://doi.org/10.1103/PhysRevA.69.052505

[9] Ito, Y., Tochio, T., Oohashi, H., Vlaicu, A. M., 2006. Contribution of the [1s3d] shake process to $K\alpha_{1,2}$ spectra in 3d elements. Rad. Phys. Chem. 75, 1534. https://doi.org/10.1016/j.radphyschem.2005.10.023

[10] Diamant, R., Huotari, S., Hämäläinen, K., Sharon, R., Kao, C. C., and Deutsch, M., 2006. The evolution of inner-shell multielectronic X-ray spectra from threshold to saturation for low- to high-Z atoms. Rad. Phys. Chem. 75, 1434. https://doi.org/10.1016/j.radphyschem.2006.05.002

[11] Fennane, K., Dousse, J.-Cl., Hoszowska, J., Berset, M., Cao, W., Maillard, Y.-P., Szlachetko, J., Szlachetko, M., and Kavčič, M., 2009. Double K-shell ionization of Al induced by photon and electron impact. Phys. Rev. A 79, 032708. https://doi.org/10.1103/PhysRevA.79.032708

[12] Ito, Y., Tochio, T., Ohashi, H., Yamashita, M., Fukushima, S., Polasik, M., Słabkowska, K., Syrocki, Ł., Szymańska, E., Rzadkiewicz, J., Indelicato, P., Marques, J. P., Martins, M. C., Santos, J. P., and Parente, F., 2016. "$K\alpha_{1,2}$ x-ray linewidths, asymmetry indices, and [KM] shake probabilities in elements Ca to Ge and comparison with theory for Ca, Ti, and Ge,". Phys. Rev. A 94, 042506. https://doi.org/10.1103/PhysRevA.94.042506

[13] Ito, Y., Tochio, Yamashita, M., Fukushima, S., Vlaicu, A. M., Syrocki, Ł., Słabkowska, K., Węder, E., Polasik, M., Sawicka, K., Indelicato, P., Marques, J. P., Sampaio, J. M., Guerra, M., Santos, J. P., and Parente, F., 2018. "Structure of high-resolution $K\beta_{1,3}$ x-ray emission spectra for the elements from Ca to Ge,". Phys. Rev. A 97, 052505. https://doi.org/10.1103/PhysRevA.97.052505

[14] Ito, Y., Tochio, Yamashita, M., Fukushima, S., Vlaicu, A. M., Marques, J. P., Sampaio, J. M., Guerra, M., Santos, J. P., Syrocki, Ł., Słabkowska, K., Węder, E., Polasik, M., Rzadkiewicz, J., Indelicato, P., Ménesguen, Y., Lépy, M.-Ch., and Parente, F., 2020. "Structure of $K\alpha_{1,2}$- and $K\beta_{1,3}$- emission x-ray spectra for Se, Y and Zr," Phys. Rev. A 102, 052820. https://doi.org/10.1103/PhysRevA.102.052820

[15] Kauffman, R. L., McGuire, J. H., Richard, P., and Moore, C. F., 1973. "Projectile and Target Dependence of the $K\alpha$ Satellite Structure". Phys. Rev. A 8, 1233. https://doi.org/10.1103/PhysRevA.8.1233

[16] Li, T. K., Watson, R. L., and Hansen, J. S., 1973. "Simultaneous K-Plus-L-Shell Ionization in Light-Ion-Atom Collisions". Phys. Rev. A 8, 1258. https://doi.org/10.1103/PhysRevA.8.1258

[17] Watson, R. L., Jenson, F. E., and Chiao, T., 1974 "Z dependence of $K\alpha$ x-ray satellite structure in heavy-ion—atom collisions". Phys. Rev. A 10, 1230. https://doi.org/10.1103/PhysRevA.10.1230

[18] Dutkiewitcz, V., Bakhru, H., and Cue, N., 1976. "$K\alpha$ x-ray satellite intensities with proton impact on Al to Fe at a fixed scaled velocity" Phys. Rev. A 13, 306. https://doi.org/10.1103/PhysRevA.13.306

[19] Hill, K. W., Doyle, B. L., Shafroth, S. M., Madison, D. H., and Deslattes, R. D., 1976. "Projectile charge and energy dependence of titanium K x rays and satellites following excitation by fast heavy ions". Phys. Rev. A 13, 1334. https://doi.org/10.1103/PhysRevA.13.1334

[20] Watson, R. L., Sonobe, B. I., Demarest, J. A., and Langenberg, A., 1979. "Systematics of the average L-shell ionization probability in K-shell ionizing collisions by light ions". Phys. Rev. A 19, 1529. https://doi.org/10.1103/PhysRevA.19.1529

[21] Perny, B., Dousse, J .-Cl, Gasser, M., Kern, J., Rhême, Ch., Rymuza, P., and Sujkowski, Z., 1987. "High-resolution study of heavy-ion-induced $K\alpha$ x-ray spectra of molybdenum atoms", Phys. Rev. A 36, 2120. https://doi.org/10.1103/PhysRevA.36.2120

[22] Boschung, B., Carlen, M. W., Dousse, J.-Cl., Galley, B., Herren, Ch., Hoszowska, J., Kern, J., Rhême, Ch., Ludziejewski, T., Rymuza, P., Sujkowski, Z., and Halabuka, Z., 1995. "Probabilities for L-shell ionization in intermediate-velocity collisions of medium-mass elements with $^4He^{2+}$ ions", Phys. Rev. A 52, 3889. https://doi.org/10.1103/PhysRevA.52.3889

[23] Kavčič, M., Šmit, Ž., Budnar, M., and Halabuka, Z., 1997. " L-shell ionization in near-central collisions of MeV protons with low-Z atoms", Phys. Rev. A 56, 4675. https://doi.org/10.1103/PhysRevA.56.4675

[24] Kavčič, M., Budnar, M., Muhleisen, A., Pelicon, P., Šmit, Ž., Žitnik, M., Castella, D., Corminboeuf, D., Dousse, J.-Cl., Hoszowska, J., Raboud, P. A., and Tökési, K., 2000. "L-shell ionization in near-central collisions of heavy ions with low-Z atoms", Phys. Rev. A 61, 052711. https://doi.org/10.1103/PhysRevA.61.052711

[25] Kavčič, M., 2003. "$K\alpha$ x-ray satellite lines of Si induced in collisions with 1–3-MeV proton". Phys. Rev. A 68, 022713. https://doi.org/10.1103/PhysRevA.68.022713

[26] Parratt, L. G., 1936. "Excitation Potential, Relative Intensities and Wave-Lengths of the $K\alpha''$ X-Ray Satellite Line", Phys. Rev. 49, 502. https://doi.org/10.1103/PhysRev.49.502

[27] Parratt, L. G., 1936. "$K\alpha$ Satellite Lines", Phys. Rev. 50, 1. https://doi.org/10.1103/PhysRev.50.1

[28] Fischer, D. W., and Baun, W. L., 1965. "Diagram and

Nondiagram Lines in K Spectra of Aluminum and Oxygen from Metallic and Anodized Aluminum". J. Appl. Phys. 36, 534. https://doi.org/10.1063/1.1714025

[29] Mikkola, E., Keski-Rahkonen, O., Lahtinen, J., and Reinikainen, K., 1983. "Determination of the $KL^2 \rightarrow L^3$ X-Ray Multiplet Structure in Na, Mg, and Al", Phys. Scr. 28, 188. https://doi.org/10.1088/0031-8949/28/2/008

[30] Misra, U. D., and Watson, L. M., 1987. "$K\alpha$ X-rays from magnesium, some of its compounds and alloys". Phys. Scr. 36, 673. https://doi.org/10.1088/0031-8949/36/4/010

[31] Salem, S. I., and Scott, B. L., 1987. "$K\alpha$ satellites of Ti, V, Fe, and Co". Phys. Rev. A 35, 1607. https://doi.org/10.1103/PhysRevA.35.1607987.

[32] Deutsch, M., Hölzer, G., Härtwig, J., Wolf, J., Fritsch, M., and Förster, E., 1995. "$K\alpha$ and $K\beta$ x-ray emission spectra of copper," Phys. Rev. A 51, 283. https://doi.org/10.1103/PhysRevA.51.283

[33] Hölzer, G., Fritsch, M., Deutsch, M., Härtwig, J., and Förster, E., 1997. "$K\alpha_{1,2}$ and $K\beta_{1,3}$ x-ray emission lines of the 3d transition metals,", Phys. Rev. A 56, 4554. https://doi.org/10.1103/PhysRevA.56.4554

[34] Limandri, S. P., Bonetto, R. D., Carreras, A. C., and Trincavelli, J. C., 2010. "$K\alpha$ satellite transitions in elements with $12 \leq Z \leq 30$ produced by electron incidence", Phys. Rev. A 82, 032505. https://doi.org/10.1103/PhysRevA.82.032505

[35] Grant, I. P., 1984. "Relativistic atomic structure theory: Some recent work", Int. J. Quantum Chem. 25, 23. https://doi.org/10.1002/qua.560250104

[36] Dyall, K. G., Grant, I. P., Johnson, C. T., Parpia, F. A., and Plummer, E. P., 1989. "GRASP: A general-purpose relativistic atomic structure program", Comput. Phys. Commun. 55, 425. https://doi.org/10.1016/0010-4655(89)90136-7

[37] Polasik, M., 1989. "Theoretical multiconfiguration Dirac-Fock method study on the x-ray spectra of multiply ionized heavy atoms: The structure of the $K\alpha$ L^n lines", Phys. Rev. A 39, 616. https://doi.org/10.1103/PhysRevA.39.616

[38] Polasik, M., 1989. "Theoretical simulation of the x-ray spectra of multiply ionized heavy atoms: The $K\alpha$ L^n spectra of molybdenum", Phys. Rev. A 39, 5092. https://doi.org/10.1103/PhysRevA.39.5092

[39] Polasik, M., 1989. "Theoretical multiconfiguration Dirac-Fock method study on the x-ray spectra of multiply ionized heavy atoms: The structure of the $K\alpha L^0 M^r$ lines", Phys. Rev. A 40, 4361. https://doi.org/10.1103/PhysRevA.40.4361

[40] Polasik, M., 1990. "Theoretical multiconfiguration Dirac-Fock method study on the x-ray spectra of multiply ionized heavy atoms: The structure of the $K\alpha L^1 M^r$ satellite lines", Phys. Rev. A 41, 3689. https://doi.org/10.1103/PhysRevA.41.3689

[41] Polasik, M., 1995. "Systematic multiconfiguration Dirac-Fock study of the x-ray spectra accompanying the ionization in collision processes: The structure of the $K\beta_{1,3} L^0 M^r$ lines", Phys. Rev. A 52, 227. https://doi.org/10.1103/PhysRevA.52.227

[42] Polasik, M., 1998. "Influence of changes in the valence electronic configuration on the $K\beta$-to-$K\alpha$ x-ray intensity ratios of the 3d transition metals", Phys. Rev. A 58, 1840. https://doi.org/10.1103/PhysRevA.58.1840

[43] Parpia, F. A., Froese Fischer, C., and Grant, I. P., 1996. "GRASP92: A package for large-scale relativistic atomic structure calculations", Comp. Phys. Commun. 94, 249. https://doi.org/10.1016/0010-4655(95)00136-0

[44] Jönsson, P., He, X., Froese Fischer, C., and Grant, I. P., 2007. "The grasp2K relativistic atomic structure package", Comp. Phys. Commun. 177, 597. https://doi.org/10.1016/j.cpc.2007.06.002

[45] Polasik, M., Słabkowska, K., Rzadkiewicz, J., Kozioł, K., Starosta, J., Wiatrowska-Kozioł, E., Dousse, J.-Cl., and Hoszowska, J., 2011. "$K^h\alpha_{1,2}$ X-Ray Hypersatellite Line Broadening as a Signature of K-Shell Double Photoionization Followed by Outer-Shell Ionization and Excitation", Phys. Rev. Lett. 107, 073001. https://doi.org/10.1103/PhysRevLett.107.073001

[46] Desclaux, J. P., 1975. "A multiconfiguration relativistic Dirac-Fock program", Comp. Phys. Commun. 9, 31. https://doi.org/10.1016/0010-4655(75)90054-5

[47] Indelicato, P., 1995. "Projection operators in multiconfiguration Dirac-Fock calculations: Application to the ground state of heliumlike ions", Phys. Rev. A 51, 1132. https://doi.org/10.1103/PhysRevA.51.1132

[48] Löwdin, P.-O., 1955. "Quantum Theory of Many-Particle Systems. I. Physical Interpretations by Means of Density Matrices, Natural Spin-Orbitals, and Convergence Problems in the Method of Configurational Interaction", Phys. Rev. 97, 1474. https://doi.org/10.1103/PhysRev.97.1474

[49] Kozioł, K., 2014. "MCDF-RCI predictions for structure and width of $K\alpha_{1,2}$ x-ray line of Al and Si,", J. Quant. Spectr. Radiat. Transf. 149, 138. https://doi.org/10.1016/j.jqsrt.2014.08.009

[50] Martins, M. C., Costa, A. M., Santos, J. P., Parente, F., and Indelicato, P., 2004. "Relativistic calculation of two-electron one-photon and hypersatellite transition energies for $12 \leq Z \leq 30$ elements", J. Phys. B: At. Mol. Opt. Phys. 37, 3785. https://doi.org/10.1088/0953-4075/37/19/001

[51] Tochio, T., Ito, Y., and Omote, K., 2002. "Broadening of the x-ray emission line due to the instrumental function of the double-crystal spectrometer", Phys. Rev. A 65, 042502. https://doi.org/10.1103/PhysRevA.65.042502

[52] Bearden, J. A., 1967. "X-Ray Wavelengths", Rev. Mod. Phys. 39, 78. https://doi.org/10.1103/RevModPhys.39.78

[53] Cauchois Y., and Sénémaud, C., 1978. "Wavelengths of X-Ray Emission Lines and Absorption Edges". Pergamon press, Oxford, 1978.

[54] Schweppe, J., Deslattes, R. D., Mooney, T. and Powell, C. J., 1994. "Accurate measurement of Mg and Al $K\alpha_{1,2}$ X-ray energy profiles", J. Electron Spectrosc. Relat. Phenom. 67, 463. https://doi.org/10.1016/0368-2048(93)02059-U

[55] Campbell, J. L., and Papp, T., 2001. "Widths of atomic K-N7 levels", At. Data and Nucl. Data Tables 77, 1. https://doi.org/10.1006/adnd.2000.0848

[56] Guerra, M., Sampaio, J. M, Vília, G. R., Godinho, C. A., Pinheiro, D., Amaro, P., Marques, J. P., Machado, J., Indelicato, P., Parente, F., and Santos, J. P.*. "Fundamental Parameters Related to Selenium $K\alpha$ and $K\beta$ Emission X-ray Spectra", Atoms 2021, 9, 8. https://doi.org/10.3390/atoms9010008

[57] Deslattes, R. D., Kessler, E. G., Indelicato, P., Billy de, L., Lindroth, E. and Anton, J., 2003. "X-ray transi-

tion energies: new approach to a comprehensive evaluation", Rev. Mod. Phys. 75, 35. https://doi.org/10.1103/RevModPhys.75.35

[58] Krause, M. O., and Oliver, J. H., 1979. "Natural Widths of Atomic K and L level, $K\alpha$ X-Ray Lines and Several KLL Auger Lines", J. Phys. And Chem. Ref. Data, 8, 329. https://doi.org/10.1063/1.555595

[59] Utriainen, J., Linkoaho, M., Rantavuori, E., Åberg, T., and Graeffe, G., 1968. "Relative Intensities of $K\alpha$ Satellites in X-Ray Fluorescence Spectra of Na, Mg, Al and Si", Zeitschrift für Naturforschung A 23, 1178. https://doi.org/10.1515/zna-1968-0812

[60] Parthasaradhi, K., Babu, G. R., Murty, V. R. K., Murti, M. V. R., and Rao, K. S., 1987. "$K\alpha$ X-ray satellite spectrum of Mg excited by photons", Nucl. Instrum. Methods Phys. Res. A 255, 54. https://doi.org/10.1016/0168-9002(87)91072-2

[61] Mauron, O., Dousse, J.-Cl., Hoszowska, J., Marques, J. P., Parente, F., and Polasik, M., 2000. "L-shell shake processes resulting from 1s photoionization in elements $11 \leq Z \leq 17$", Phys. Rev. A 62, 062508. https://doi.org/10.1103/PhysRevA.62.062508

[62] Baun, W. L., and Fischer, D. W., 1964. "The effect of valence and Coordination of K series diagram and non-diagram lines of magnesium, aluminum, and silicon", Advances in X-ray analysis 8, 371. https://doi.org/10.1154/S037603080000327X

[63] Krause, M. O., and Ferreira, J. G., 1975. "K X-ray emission spectra of Mg and Al", J. Phys. B: At. Mol. Opt. Phys. 8, 2007. https://doi.org/10.1088/0022-3700/8/12/013

[64] Mauron, O., and Dousse, J.-Cl., 2002. "Double KL ionization in Al, Ca, and Co targets bombarded by low-energy electrons", Phys. Rev. A 66, 042713. https://doi.org/10.1103/PhysRevA.66.042713

[65] Åberg, T., 1968. "X-ray satellite intensities in the sudden approximation", Phys. Lett. A 26, 515. https://doi.org/10.1016/0375-9601(68)90823-2

[66] Bearden, J. A., and Burr, A. F. 1967. "Reevaluation of X-Ray Atomic Energy Levels", Rev. Mod. Phys. 39, 125 https://doi.org/10.1103/RevModPhys.39.125

[67] Carlson, T. A., and Nestor, C. W., Jr, 1973. "Calculation of Electron Shake-Off Probabilities as the Result of X-Ray Photoionization of the Rare Gases", Phys. Rev. A 8 2887. https://doi.org/10.1103/PhysRevA.8.2887

[68] Kas, J. J., Rehr, J. J., and Curtis, J. B., 2016. "Particle-hole cumulant approach for inelastic losses in x-ray spectra", Phys. Rev. B 94 035156. https://doi.org/10.1103/PhysRevB.94.035156

[69] Esteva, J. M., Gauthe, B., Dhez, P., and Karnatak, R. C., 1983. "Double excitation in the K absorption spectrum of neon", J. Phys. B: Atom. Mol. Phys. 16, L263. https://doi.org/10.1088/0022-3700/16/9/003

[70] Deslattes, R. D., LaVilla, R. E., Cowan, P. L., and Henins, A., 1983. "Threshold studies of a multivacancy process in the $K\beta$ region of argon", Phys. Rev. A 27, 923. https://doi.org/10.1103/PhysRevA.27.923

[71] Deutsch M., and Hart, M., 1986. "Multielectron X-Ray Photoexcitation Measurements in Krypton", Phys. Rev. Lett. 57, 1566. https://doi.org/10.1103/PhysRevLett.57.1566

[72] Zhang, K., Stern, E. A., Rehr, J. J., and Ellis, F., 1991. "Double electron excitation in atomic Xe", Phys. Rev. B 44, 2030. https://doi.org/10.1103/PhysRevB.44.2030

[73] Rehr, J. J., and Albers, R. C., 2000. "Theoretical approaches to x-ray absorption fine structure", Rev. Mod. Phys. 72, 621. https://doi.org/10.1103/RevModPhys.72.621

[74] Gomilšek Padežnik, J., Kodre, A., Arčon, I., Loireau-Lozac'h, A. M., and Bénazeth, S., 1999. "Multielectron photoexcitations in x-ray-absorption spectra of 4p elements", Phys. Rev. A 59, 3078. https://doi.org/10.1103/PhysRevA.59.3078

[75] Ménesguen, Y., Gerlach, M., Pollakowski, B., Unterumsberger, R., Haschke, M., Beckhoff, B., and Lépy, M.-C., 2016. "High accuracy experimental determination of copper and zinc mass attenuation coefficients in the 100 eV to 30 keV photon energy range", Metrologia 53, 7. https://doi.org/10.1088/0026-1394/53/1/7

[76] Ménesguen, Y., Lépy, M.-C., Hönicke, P., Müller, M., Unterumsberger, R., Beckhoff, B., Hoszowska, J., Dousse, J.-Cl., Błachucki, W., Ito, Y., Yamashita, M., and Fukushima, S., 2018. "Experimental determination of the x-ray atomic fundamental parameters of nickel", Metrologia 55, 56. https://doi.org/10.1088/1681-7575/aa9b12

[77] Ménesguen, Y., Lépy, M.-C., Sampaio, J. M., Marques, J. P., Parente, F., Guerra, M., Indelicato, P., Santos, J. P., Hönicke, P., and Beckhoff, B., 2018. "A combined experimental and theoretical approach to determine X-ray atomic fundamental quantities of tin", X-Ray Spectrometry 47, 341. https://doi.org/10.1002/xrs.2948

[78] Ménesguen, Y., and Lépy, M.-C., 2010. "Mass attenuation coefficients in the range $3.8 \leq E \leq 11$ kev, K fluorescence yield and K_β/K_α relative X-ray emission rate for Ti, V, Fe, Co, Ni, Cu, and Zn measured with a tunable monochromatic X-ray source", Nucl. Instrum. Methods Phys. Res. B 268, 2477. https://doi.org/10.1016/j.nimb.2010.05.044

[79] JCGM, *Evaluation of measurement data - Guide to the expression of uncertainty in measurement*. BIPM, 2008, consultation date: 2015. [Online]. Available: http://www.bipm.org/fr/publications/guides/gum.html

[80] Cullen, D. E., Hubbell, J. H.. and Kissel, L., 1997. "EPDL97: the Evaluated Photon Data Library, '97 Version"", *UCRL-50400*, vol. 6, no. 5, 1997, consultation date: 2017. [Online]. Available: https://www-nds.iaea.org/epdl97/document/epdl97.pdf

[81] Ravel B., and Newville, M., 2005. "ATHENA, ARTEMIS, HEPHAESTUS: data analysisfor X-ray absorption spectroscopy using IFFEFIT", J. Synchrotron Rad. 12, 537. https://doi.org/10.1107/S0909049505012719

[82] Victoreen, J. A., 1949. "The Calculation of X-Ray Mass Absorption Coefficients", J. Appl. Phys. 20, 1141. https://doi.org/10.1063/1.1698286

[83] Froese Fischer, C., 1987. "General Hartree-Fock Program", Comput. Phys. Commun. 43, 355. https://doi.org/10.1016/0010-4655(87)90053-1